Mechanical Systems and Signal Processing 177 (2022) 109185

Contents lists available at ScienceDirect

Mechanical Systems and Signal Processing

journal homepage: www.elsevier.com/locate/ymssp

A cantilever-type vibro-impact triboelectric energy harvester for wind energy harvesting

Chaoyang Zhao, Guobiao Hu, Yaowen Yang *

School of Civil and Environmental Engineering, Nanyang Technological University, 50 Nanyang Avenue, 639798, Singapore

ARTICLE INFO

Communicated by Daniil Yurchenko

Keywords:
Triboelectric energy harvester
Wind energy
Galloping effect
Distributed aero-electro-mechanical model
Impact effect

ABSTRACT

This paper presents a novel wind energy harvester utilizing galloping effect coupled with triboelectric-based energy conversion to convert the flow-induced structural vibration into electricity. The proposed harvester comprises a host cantilever beam, a stopper, and a middle plate with one rotation degree of freedom. The triboelectric layers and electrodes are placed in between the surface of the stopper and middle plate. A bluff body is fixed at the free end of the host beam to induce galloping vibration, which drives the middle plate to contact with the stopper periodically, thus generating electricity due to the triboelectric-based conversion mechanism. The proposed harvester can harness energy from wind velocity as low as 2 m/s depending on the selection of cantilever beams. A distributed coupled aero-electro-mechanical model is formulated to investigate the dynamic behavior of the harvester. The impact between the middle plate and stopper is found to have a significant influence on the energy generation performance of the harvester. Rigid impact could cause irregular and impulsive separation of contact surfaces, leading to sporadic voltage output. An optimal configuration is determined by selecting proper parameters of the stopper, bluff body, and gap distance in the design of the harvester. The proposed model shows good accuracy for modeling a moderate impact-engaged triboelectric harvester working on contact and separation mode. The fabricated harvester prototypes can produce a root mean square voltage of 12.8 V with a maximum power of 290 μW at wind velocity of 10 m/s. Even at low wind velocity, such as 6 m/s, the maximum power can reach up to 196 μW, demonstrating the promising energy scavenging capability of the proposed harvester.

1. Introduction

As a renewable and clean energy source, wind power generation has attracted extensive research attentions. For small-scale energy harvesting that aims to power electronic devices, many energy harvesters have been proposed based on various energy conversion mechanisms to convert wind energy into electricity. One typical example is the wind turbine that is designed based on electromagnetic energy conversion. Aerodynamic-induced vibration has long been a major concern in the design of high-rise buildings and aircraft. However, from the energy harvesting point of view, such vibration is an ideal energy source that can be converted into electricity. Piezoelectric materials have attracted much attention for their abilities to convert mechanical vibration into electricity [1,2]. They have been used by many researchers to harness energy from ambient wind-induced vibrations [3–5]. However, piezoelectric materials are usually very brittle, which will cause structural fatigue in long-term operations. In recent years, triboelectric energy harvesters (TEH) have emerged as suitable alternatives for energy conversion due to their merits of wide materials availability, lightweight, low

* Corresponding author.

https://doi.org/10.1016/j.ymssp.2022.109185
Received 29 December 2021; Received in revised form 5 March 2022; Accepted 16 April 2022
Available online 23 April 2022

cost, and high efficiency even at low frequencies [6–8]. The basic component of TEH is usually called tribo-pair, which consists of triboelectric materials and electrodes.

Rotary-based structures widely exist in the design of triboelectric wind energy harvesters. For example, *Shun et al.* [9] reported a broadband TEH based on a dual-rotation shaft. The harvesting system contains two sets of coaxial wind cups with diverse arm lengths, and each of them has its own rotation shaft. Energy harvesting modules are constructed on the outer and inner rotors. The wind drives the rotation of the wind cups, which results in the sliding between triboelectric material and electrodes, thus generating electricity from the rotation of the rotors. The harvester can collect energy from a broad wind velocity range from 2.2 m/s to 16 m/s. *Wang et al.* [10] and *Zhao et al.* [11] also reported similar rotary structures in wind energy harvester design. *Bu et al.* [12] proposed a TEH working on the contact-sliding-separation mode. The device consisted of rigid rotors coupled to the shaft and flexible stators arranged in a circle. With three rotors and four stators, an average power of 1.04 W was obtained for the loading resistance of 511 Ω at 563 rpm. Their design boosted the power output to a higher level than the traditional sliding mode TEH. Rotary-based TEH is usually massive and requires a complex manufacturing process. Once the fabrication is completed, replacing the components will become troublesome, which might be the limitation for rotary-based TEHs.

Flutter effect also attracts much attention in the design of TEHs. Fluttering is a common aerodynamic effect in daily life, like the flags blowing in the wind. *Bae et al.* [13] proposed a flutter-driven TEH using a flexible flag and a rigid plate. The flag coated with golden metal worked as the fluttering body as well as an electrode. Polytetrafluoroethylene (PTFE) film was attached to the surface of the rigid plate. Their interaction generated periodic contact and separation, leading to an alternating current (AC) output. The harvester produced a maximum voltage of 250 V and a current of 70 μA at a wind velocity of 22 m/s. *Zhang et al.* [14] reported a lawn structured TEH aiming at sweeping wind energy on rooftops. The basic unit of the harvester was a pair of strips comprising indium tin oxide (ITO) coated polyethylene terephthalate (PET) with one end fixed to the substrate and the other end stayed free-standing. The wind flow induced the contact between pairs. With a unit number of 60, the harvester exhibited a rooftop power density of 2.37 W/m^2 at the wind velocity of 27 m/s. Similar designs can also be found in the works from *Perez et al.* [15,16] and *Phan et al.* [17]. The vibration frequency of the structure due to flutter is usually high. Therefore, flutter-based energy harvesters usually require a high wind velocity to stimulate, which restricts the practical application of this type harvester since high-speed winds are rare in our ambient environments [18,19].

In addition to the flutter, galloping is also an ideal aerodynamic effect that is utilized in many harvester designs. Galloping effect is a type of self-excited aerodynamic phenomenon that gives increasing amplitude oscillations of the bluff body when subjected to growing wind flows. Many works have employed such an effect in the design of piezoelectric energy harvesters [20–22]. However, only a few recent works design wind energy harvesters using triboelectric materials by leveraging the galloping effect. For instance, *Zhang et al.* [23] constructed a two-beam structure with one beam attached with a Y-shaped bluff body. The tribo-pair was constructed on two square substrates placed between the two beams near the bluff body. The harvester achieved a very low cut-in wind velocity of 1.4 m/s, and the voltage output could reach 200 V. *Wang et al.* [24] attached a C-shaped bluff body to a cantilever beam and proposed symmetric geometric boundaries that were 3D-printed with a curved surface. The geometric boundaries clamped the cantilever beam with the tribo-pair constructed between the curved faces and the surface of the beam. The harvester could generate a total power output of around 135 μW at a wind speed of 14 m/s. Besides, the harvester also showed the capability of integrating with a piezoelectric patch to further increase the energy conversion efficiency. Those works are good demonstration of utilizing the galloping effect in the TEH design. It is worthwhile to devote more efforts in improving the design of galloping triboelectric energy harvesters, aiming at their practical applications of powering small electronics and wireless sensors.

Electrical modeling for fundamental TEH with parallel contact surfaces has been well established [25–27]. However, few works have been devoted to the coupled electro-mechanical modeling of TEHs considering the dynamic behavior of the harvester structure, especially when the impact is engaged in the model. Using a piecewise linear system is common in dealing with the impact in the mathematical modeling of lumped parameter models. An additional stiffness is added into the system to simulate the impact behavior when it happens. For example, *Ibrahim et al.* [28] developed a coupled electro-mechanical model based on the piecewise impact for a harvester working in contact and separation mode. The simulated results showed good agreement with the experimental results, which provided some insights on surface charge generation influence by impact. *Fu et al.* [29] presented a TEH in the form of a vibro-impact system with three cantilever beams. The impact was modeled by considering the just-before-impact velocity and the velocity-dependent coefficient. In addition to impact modelling, current modeling concerning aerodynamic force was based on the lumped parameter method, which might lose the accuracy for the model prediction [23,24]. A distributed model is thus desired for precise modeling, especially when the aerodynamic force and impact are involved simultaneously.

Owing to the excellent design flexibility of the cantilever beam, this work proposes a cantilever-type galloping energy harvester using triboelectric materials (GTEH). An aero-electro-mechanical model considering the aerodynamic force and the impact is established to analyze the mechanical and electrical properties of the GTEH. Prototypes of the proposed GTEH are fabricated for wind tunnel tests, and the model is validated experimentally. The rest of this paper is organized as follows. Section 2 introduces the harvester structure design and working mechanism. The aero-electro-mechanical model is discussed in detail in Section 3. Section 4 presents the experimental setup. Preliminary experimental results and model validation are presented in Section 5. Optimization of the harvester through a parametric study based on the preliminary results is addressed in Section 6. In Section 7, the performance demonstration of the harvester is presented, followed by conclusions in the last section.

2. Structure design

The proposed GTEH consists of a host cantilever beam, a bluff body, a mechanical stopper, and a tribo-pair. As shown in Fig. 1, the

host beam and stopper are attached in parallel at the left side with a middle plate being placed in between. The middle plate is connected to the spacer by an elastomer that allows the middle plate to rotate along the fixed end when the host beam vibrates. The triboelectric pair that consists of a PTFE film, a copper, and an aluminum foil is configured between the stopper and middle plate. A flexible tape connects the support of the middle plate to the host beam. One bluff body is mounted at the free end of the host beam. The cross-sectional shapes of bluff bodies dominate the transverse galloping effect. There are different types of bluff bodies, like D-shape [30], square-shape [31,32], triangle-shape [33], and Y-shape [20], in which the square cross-section of the bluff body is a typical design that has demonstrated outstanding performance for transverse galloping energy harvesting. Meanwhile, there is a fully validated aerodynamic model to estimate the galloping force of the square bluff body, which can facilitate establishing the aero-electro-mechanical model for the proposed GTEH [34–36].

When the bluff body is exposed to wind flow, it vibrates once the wind velocity exceeds a critical threshold, i.e., the cut-in wind velocity. The vibration of the host beam makes the middle plate approach to and depart from the stopper. Owing to the tribo-electrification, negative charges are generated at the surface of the PTFE film, and positive charges are accumulated at the surface of the copper electrode when the tribo-pair is in contact. When the tribo-pair separates, the change of the established electrical potential drives the negative charges flow from the aluminum electrode to the copper electrode until the electrical potential equilibrium is reached due to the electrostatic induction. When the tribo-pair approaches each other again, the negative charge flows in a reverse way, i.e., from the copper electrode to the aluminum electrode. Therefore, the charge can flow back and forth through the external circuit with the periodic vibration of the host beam to generate an alternating current (AC). In a word, the electrostatic charge generates at the material surface because of the triboelectrification. Furthermore, the electrostatic induction drives the charge flow through the external circuit. In this way, the mechanical vibration energy of the host beam is converted into electricity from the frequent contact and separation of the tribo-pair.

3. Aero-electro-mechanical model

3.1. Mechanical model

The formulation of an analytical model is crucial for thoroughly investigating the dynamic behavior of the harvester and further guiding the design optimization of GTEH. The lump parameter model is quite common in TEH modeling, which has some accuracy in terms of power prediction. For precise modeling, a distributed model is desired. In our case, the model should consider the electro-mechanical coupling effect between the triboelectric pair and the cantilever beam, and the interaction between the wind flow and the bluff body. Besides, according to our previous work [37], the non-parallel configuration of the triboelectric layer has to be taken into account as well. Impact happens when the middle plate contacts with the stopper. There are three principal methods in dealing with the impact in the model. (1) In the force integration method (FIM), the contact force is proportional to the penetration distance of the beam at the impact location [38,39]. (2) For the mode switch method (MSM), the mode shapes of the continuous beam are re-evaluated when it is in contact with the obstacle, and they are also treated as the basis for representing the motion of the beam during impact [40,41]. (3) Coefficient of restitution (CoR) method treats the obstacle to be rigid and uses the CoR assumption to evaluate the states of the beam before and after the impact [42,43]. Overall, the MSM requires the generation of the mode shapes for the beam when it is in contact with the obstacle. The FIM introduces the impact force into the equation without changing the initial mode of the continuous beam, which is more straight-forward as compared to the MSM. The CoR method is always used to solve the problem with rigid impact. In this study, the most general FIM is employed to deal with the impact of the vibro-impact beam.

In order to formulate the mathematical model of the harvester, necessary simplifications are adopted. As shown in Fig. 2, the proposed GTEH can be simplified as a host cantilever beam with a tip mass attached to its free end. The stopper is much stiffer than the host beam, and it can be treated as a grounded spring-damper system with a gap to the beam. The stopper is thus represented by the combination of a spring with a stiffness of k_c and an in-parallel damper with a viscous damping coefficient ofc_c. The motion of the host beam is divided into two stages. In stage 1, there is no impact between the host beam and the stopper, and the beam is only subjected to the galloping force. In stage 2, the impact force must be included in the system due to the occurrence of the impact. Based on the Euler-Bernoulli beam theory, the dynamic equation of the host beam subjected to galloping force can be given by:

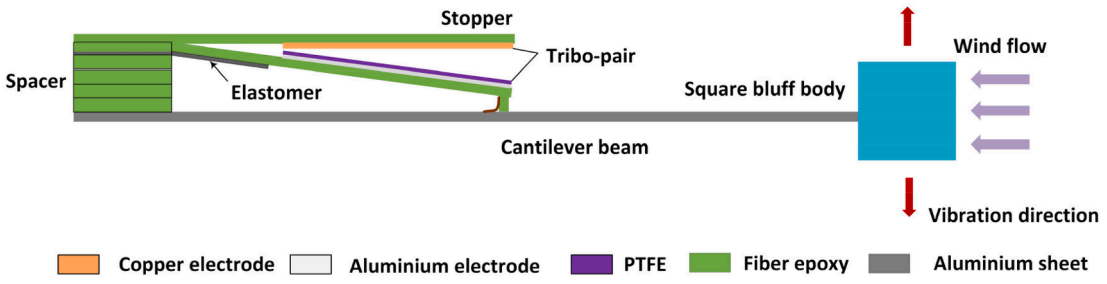

Fig. 1. Schematic diagram of the top view of the proposed GTEH.

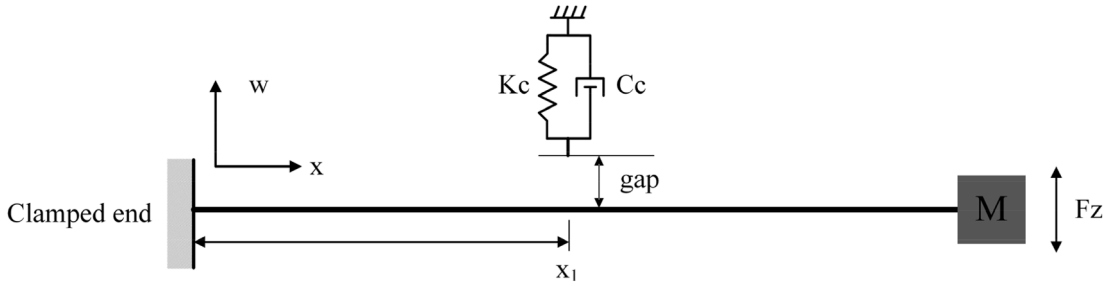

Fig. 2. Schematic diagram showing simplified model of GTEH.

$$\frac{\partial^2}{\partial x^2}\left[EI\frac{\partial^2 w(x,t)}{\partial x^2}\right]+c_s I\frac{\partial^5 w(x,t)}{\partial x^4\partial t}+c_a\frac{\partial w(x,t)}{\partial t}+m\frac{\partial^2 w(x,t)}{\partial t^2}=F_z\delta(x-L)+F_c\delta(x-x_1) \tag{1}$$

where $w(x,t)$ denotes the transverse deflection of the host beam. E is the Young's modulus, and I is the area moment of inertia of the beam cross-section. c_s and c_a are the strain damping and viscous air damping, respectively [44,45]. m is the distributed mass of the beam. According to the quasi-static assumption [34], the galloping force F_z is expressed as:

$$F_z=\frac{1}{2}\rho hlU^2\sum_{i=1}^{3}A_i\alpha^i,\alpha=\frac{\dot{w}(L,t)}{U}+w'(L,t) \tag{2}$$

in which, the dot and prime represent the differentiation with respect to time and location, respectively.ρ,h, l and U are, respectively, the air density, the height of the bluff body, the length of the bluff body, and the wind velocity. $w'(L,t)$ denotes the rotation angle of the beam at its free end, and L is the length of the host beam. For the bluff body with a square cross-section, a cubic polynomial function is adopted to represent the aerodynamic force. The three coefficients of the cubic polynomial function are, respectively, $A_1 = 2.3$, $A_2 = 0$ and $A_3 = -18$. It should be noted that these values are applicable for the wind flow with a Reynolds number larger than 33,000 with zero turbulence [46], which is similar to our wind test conditions that will be discussed in the next section. Eq. (1) does not include the electrostatic force because of a relatively small amount of charges accumulated on the material surface. The electrostatic force is thus quite small, especially compared to the impact force. The impact force between the host cantilever beam and the stopper is much larger than the electrostatic force, and the impact coupling is also much stronger than the electrical coupling in the proposed harvester. Therefore, only the forward coupling (mechanical → electrical) will be considered in the proposed model. The backward coupling (electrical → mechanical) is negligible, thus not included.

When the host beam pushes the middle plate to contact the stopper, the impact force occurs and applies to the host beam. Assuming that the gap between the host beam and the stopper isg_0 , then the impact force is given by:

$$F_c=\begin{cases}0, & w(x_1,t)<g_0\\ k_c(g_0-w(x_1,t))-c_c\dot{w}(x_1,t), & w(x_1,t)\geqslant g_0\end{cases} \tag{3}$$

in which, x_1 is the location of the motion transformation point, i.e., the support. Thus,$w(x_1,t)$ and $\dot{w}(x_1,t)$ are the displacement and velocity at $x=x_1$ on the host beam, respectively. δ is the Dirac function. Using the mode superposition method, the solution of Eq. (1) can be written as follows by separating the variables:

$$w(x,t)=\sum_{r=1}^{\infty}\phi_r(x)\eta_r(t) \tag{4}$$

where $\phi_r(x)$ is the mass normalized modal shape for the r^{th} mode of the corresponding undamped free vibration case, and $\eta_r(t)$ is the modal coordinate. Substituting Eq. (4) into Eq. (1), considering all the boundary conditions, the eigenfunction expression for the r^{th} mode of a uniform clamped-free beam with tip mass can be written as [47,48]:

$$\phi_r(x)=C_r[\cos\frac{\lambda_r}{L}x-\cosh\frac{\lambda_r}{L}x+\beta_r(\sin\frac{\lambda_r}{L}x-\sinh\frac{\lambda_r}{L}x)] \tag{5}$$

where

$$\beta_r=\frac{mL(\sin\lambda_r-\sinh\lambda_r)+\lambda_r M_t(\cos\lambda_r-\cosh\lambda_r)}{mL(\cos\lambda_r+\cosh\lambda_r)-\lambda_r M_t(\sin\lambda_r-\sinh\lambda_r)} \tag{6}$$

The eigenvalues λ_r appearing in the eigenfunctions are the roots of the following characteristic equation:

$$1+\cos\lambda\cosh\lambda+\frac{\lambda M_t}{mL}(\cos\lambda\sinh\lambda-\sin\lambda\cosh\lambda)-\frac{\lambda^3 I_t}{mL^3}(\cosh\lambda\sin\lambda+\sinh\lambda\cos\lambda)+\frac{\lambda^4 M_t I_t}{m^2L^4}(1-\cos\lambda\cosh\lambda)=0 \tag{7}$$

in which, M_t and I_t are the mass and rotary inertial of the bluff body, respectively. The modal coefficient C_r of the r^{th} mode can be evaluated by considering the following orthogonality conditions:

$$\begin{aligned}&\int_0^L \phi_s(x)m\phi_r(x)dx+\phi_s(L)M_t\phi_r(L)+\left[\frac{d\phi_s(x)}{dx}I_t\frac{d\phi_r(x)}{dx}\right]_{x=L}=\delta_{rs}\\&\int_0^L \phi_s(x)EI\frac{d^4\phi_r(x)}{dx^4}dx-\left[\phi_s(x)EI\frac{d^3\phi_r(x)}{dx^3}\right]_{x=L}+\left[\frac{d\phi_s(x)}{dx}EI\frac{d^2\phi_r(x)}{dx^2}\right]_{x=L}=\omega_{nr}^2\delta_{rs}\end{aligned} \tag{8}$$

Now, substituting Eq. (4) into Eq. (1) and Eq. (3) and using the above orthogonality conditions, the governing equations of the system can be rewritten in the modal coordinate form as:

$$\ddot{\eta}_r(t)+2\zeta_r\omega_{nr}\dot{\eta}_r(t)+\omega_{nr}^2\eta_r(t)=f_z+f_c \tag{9}$$

where

$$f_z=\phi_r(L)\times\frac{1}{2}\rho hlU^2\sum_{i=1}^{3}A_i\left[\frac{\sum_{r=1}^{\infty}\phi_r(L)\dot{\eta}_r(t)}{U}+\sum_{r=1}^{\infty}\phi_r'(L)\eta_r(t)\right]^i \tag{10}$$

$$f_c=\begin{cases}0, & w(x_1,t)<g_0\\ \phi_r(x_1)[k_c(g_0-w(x_1,t))-c_c\dot{w}(x_1,t))], & w(x_1,t)\geqslant g_0\end{cases} \tag{11}$$

In Eq. (9), ζ_r is the modal damping ratio. In Eq. (8) and Eq. (9), the modal natural frequency ω_{nr} is expressed as follows:

$$\omega_{nr}=\lambda_r^2\sqrt{\frac{EI}{mL^4}} \tag{12}$$

The mechanical part model of the proposed GTEH is established by following the above procedures. In the next subsection, the electrical part model will be developed to predict the energy generation ability of the harvester.

3.2. Electrical model

Fig. 3 shows the non-parallel configuration and the electrical field distribution in between the contact surfaces. Based on the basic electrical potential equilibrium equation $V_a+V_d+V_R=0$, and the voltage equation $V(t)=RI(t)=R\cdot dQ/dt$, the governing equation for the triboelectric energy harvester with a non-parallel configuration of the contact surfaces is given as:

$$R\frac{dQ}{dt}+\frac{Q}{S\varepsilon_0}\left(\frac{d}{\varepsilon_r}+\mu g(t)\right)-\frac{\sigma\mu g(t)}{\varepsilon_0}=0,\ Q(t=0)=q_0 \tag{13}$$

where R is the external loading resistance. Q is the transferred charge between two electrodes. S represents the area of the contact surface. ε_0 is the vacuum permittivity, d is the thickness of triboelectric material, and ε_r is the relative permittivity of the triboelectric material. σ denotes the surface charge density of the triboelectric material. q_0 is the initial transferred charge. Compared to the conventional electrical model of TEH with a parallel configuration of contact surface [26,27,49], there is an additional parameter μ in

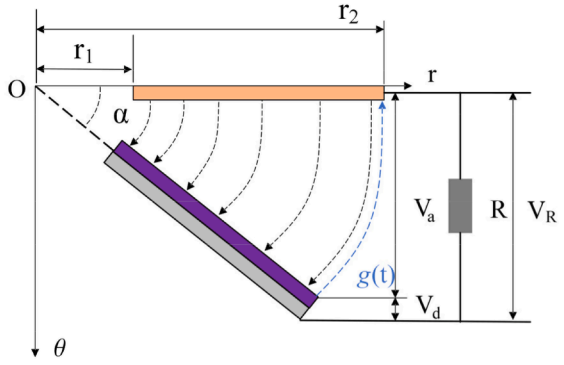

Fig. 3. Schematic of tribo-pair with non-parallel configuration.

Eq. (13) $\mu = 1/\ln(r_2/r_1)$ is relevant to the geometric parameter of the triboelectric pairs, and it can be regarded as an equivalent coefficient for the distance between two contact surfaces. r_1 and r_2 are measured from the edges of triboelectric material to the rotation center. The detailed derivation of the electrical equation can be referred to our previous work [37]. The mechanical model and electrical model are coupled together by the motion at $x = x_1$, which is $g(t) \approx g_0 - w(x_1,t)$. The coupled aero-electro-mechanical model can be solved numerically.

4. Experimental setup

This study targets on low wind velocity energy harvesting. Firstly, three harvester prototypes (GTEH-A, GTEH-B, and GTEH-C) are designed and fabricated. A proper dimension of the host beam is selected by considering its natural frequency and corresponding cut-in wind velocity when being exposed to the wind flow. Triboelectric pairs with various dimensions are attached to the host beam for the preliminary test. The bluff body is made of lightweight foam that has good cutting flexibility. Detailed properties of the three prototypes are listed in Table 1. It should be noted that the maximum gap is measured at the free end of the triboelectric pair, and it can be controlled by adjusting the thickness of the spacer. The selected gap ensures the contact between the middle plate and the stopper at relatively low wind velocity. Fig. 4 shows the experimental setup. The test is conducted in a downstream-fan type wind tunnel (FM 670 EdLabQuip) designed to study the subsonic aerodynamics. One end of the harvester is clamped at a fixture placed inside the test chamber with a dimension of 300 mm × 300 mm × 600 mm (long). The bluff body is attached at another end of the host beam, and it is exposed to the wind flow. The wind velocity could be adjusted from the controller, and the anemometer (TESTO 425) measures the wind velocity during the test, and the pitot probe of the anemometer is installed up-right to ensure accurate velocity measurement. The voltage generated from the harvester is acquired through the NI 9229 DAQ module and recorded by the SignalExpress software installed on the computer.

5. Results and discussion

The voltage output of the harvester is recorded when increasing the wind velocity. The results are given in Fig. 5. One common feature of all the prototypes is that the voltage increases with the wind velocity. The cut-in wind velocity for both GTEH-A and GTEH-B are smaller than 2 m/s, indicating that the proposed harvester is suitable for low-velocity wind energy harvesting. For GTEH-C, the cut-in wind velocity is around 5 m/s. It is noted that the length of the stopper of GTEH-C is longer than GTEH-A and GTEH-B, and its right end is very close to the bluff body, which affects the wind flow passing through the bluff body and results in the increase of cut-in wind velocity. The voltage output increases steeply after the cut-in wind velocity since increased vibration amplitude eases the contact between two triboelectric layers. A higher wind velocity makes the host beam approach the stopper with a higher speed, which benefits the charge transformation, thus giving rising of the voltage output. However, further increasing the wind velocity has little influence on the voltage output due to the limit of the total amount of charge accumulated on the surface of the triboelectric material. GTEH-C produces the highest peak-peak voltage (V_{P-P}) output of 75 V at the wind velocity of 10 m/s (Fig. 5(a)). Assuming that all the GTEHs have the same surface charge density for the material, it is no surprise that GTEH-C generates the highest output given its largest contact surface and biggest amount of charges.

Fig. 5(b) shows the root mean square (RMS) voltage (V_{RMS}) for all GTEHs. Obviously, V_{P-P} is much larger than V_{RMS}. Taking GTEH-B at wind velocity of 10 m/s as an example, V_{P-P-B} is 62 V. However, the corresponding V_{RMS-B} is only 6 V owing to the pulse-like voltage signal of triboelectric harvesters. As shown in Fig. 5(d), for a conventional harmonic sinusoidal voltage signal, the peak-to-peak and RMS voltage amplitudes are related by $V_{RMS} = \sqrt{2}/2 \cdot V_P$, in which the coefficient is evaluated considering the effectively covered area of the signal. As for the pulse-like signal from TEH (Fig. 5(c)), the covered area is much smaller than the sinusoidal one, leading to an even smaller V_{RMS} as compared to V_{P-P}. Overall, the V_{RMS} shows a similar trend as of V_{P-P} with an exception for GTEH-C. Its motion transformation support is close to the beam end, which makes the tribo-pair contact and depart faster than the other two, resulting in a short time duration of the voltage signal. Therefore, even though the V_{P-P} of GTEH-C is high, its V_{RMS} is still low. Though a large-sized stopper contributes to a large contact surface and accumulated charges, it also influences the aerodynamic characteristics of the harvester. Arbitrarily increasing the size of the stopper could possibly lead to the increase of the cut-in wind velocity and the reduction of the V_{RMS}. Thus, there is a trade-off for selecting the length of the middle plate and the stopper.

Table 1
Geometric parameters of three proposed GTEH prototypes.

Properties	GTEH-A	GTEH-B	GTEH-C
Dimensions of host cantilever beam (Aluminum) (mm × mm × mm)	0.7 × 25 × 250	0.7 × 25 × 250	0.7 × 25 × 250
Dimensions of mechanical stopper (FR4) (mm × mm × mm)	3 × 25 × 105	3 × 50 × 125	3 × 50 × 175
Dimensions of triboelectric pair (mm × mm)	25 × 80	50 × 100	50 × 150
Dimensions of bluff body (Foam) (mm × mm × mm)	40 × 40 × 150	40 × 40 × 150	40 × 40 × 150
Weight of bluff body (g)	12.5	12.5	12.5
Initial gap distance, g_0 (mm)	2	2	2

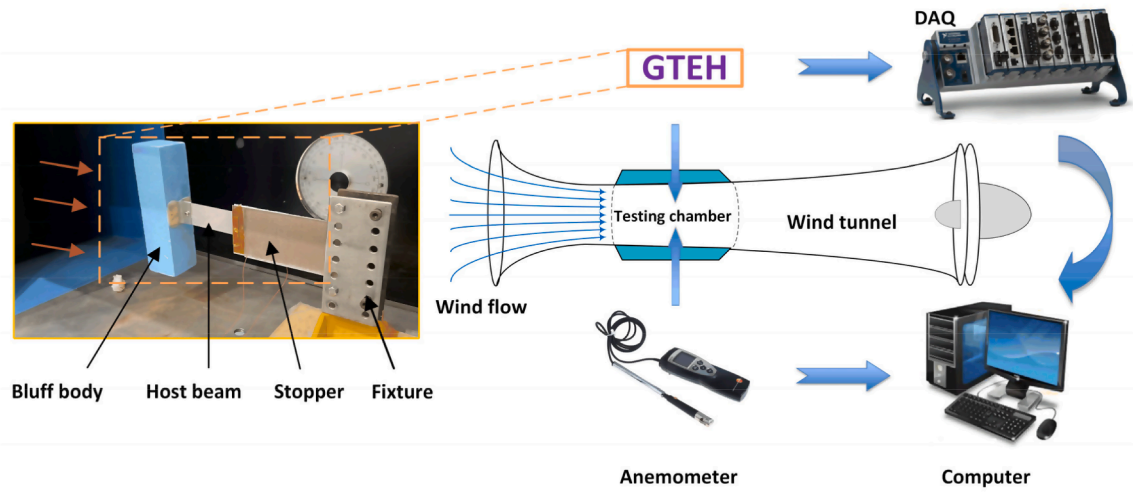

Fig. 4. Experimental setup for testing the proposed GTEH.

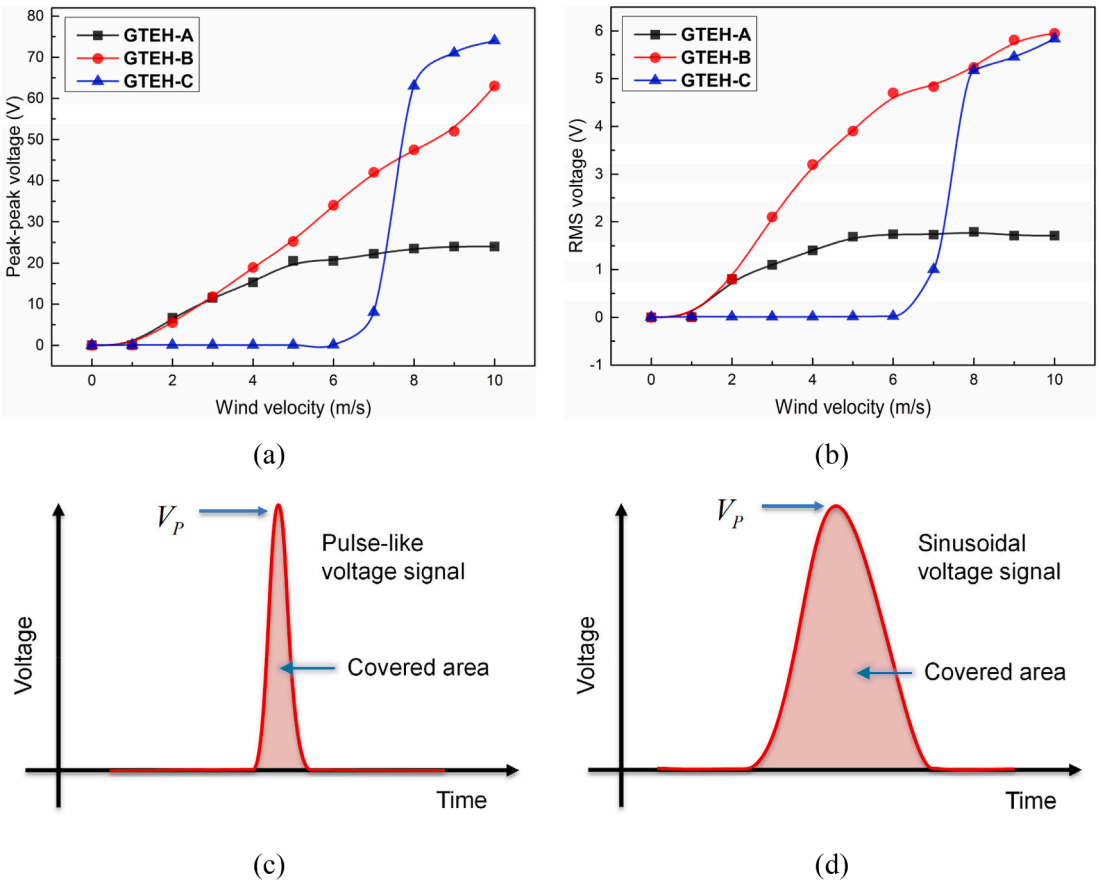

Fig. 5. Voltage output at different wind velocities: (a) Peak voltage; (b) RMS voltage; (c) pulse-like voltage signal; (d) Sinusoidal voltage signal.

Based on the above preliminary results, the harvester GTEH-A is used to validate the proposed aero-electro-mechanical model since the noticeable bending of the stopper in the experiment verifies its appropriateness of spring-damper simplification. The parameters used in the modeling are listed in Table 2. The transferred charge during contact and separation of the tribo-pair is measured by an electrometer, and the surface charge is estimated to be 3.0×10^{-5}C/m^2. The first natural frequency of the host beam is 4 Hz. In order to capture the vibro-impact behavior of the system, the first 6 mode shapes of the host beam are considered in the distributed aero-

Table 2
Parameters used in model validation for GTEH-A.

Parameters	Values
Density of host beam	2700 kg/m^3
Young's modulus of host beam	69 GPa
Air density	1.1644 kg/m^3
Location of motion transmission support, x_1	80 mm
Contact stiffness,k_c	200 N/m
Damping coefficient of stopper,c_c	0.05
Modal damping ratio,ζ_r	0.007
Vacuum permittivity,ε_0	8.854×10^{-12}F/m
Relative permittivity of PTFE,ε_r	2.1
Thickness of PTFE, d	0.1 mm
External resistance, R	1 MΩ
Equivalent coefficient, μ	0.087
Surface charge density,σ	3.0×10^{-5}C/m^2

electro-mechanical model. The wind velocity sweeps from 1 m/s to 10 m/s.

Fig. 6 shows the beam displacement at the motion transformation location ($x_1 = 80$ mm) at the wind velocity of 10 m/s. The maximum absolute displacement is larger than the maximum relative displacement when impact happens. The difference corresponds to the penetration distance of the spring-damper system. We would like to clarify that the penetration distance is defined as the tip deflection of the stopper when the host cantilever beam pushes the stopper at its free end (NOT the actual penetration between the two contact materials). There is no charge transfer in the penetration region because the tribo-pair maintains the contact status. Only the relative displacement contributes to the electrical output, and it will be substituted into the electrical model to evaluate the energy generation performance of the harvester.

Fig. 7 gives a detailed explanation of the simulated results involving the relation of the actual motion of the host beam to the charge transformation and voltage generation. In phase 1, the host beam vibrates starting from the equilibrium position with no charge transformation. Thus, no voltage output is produced during phase 1. The host beam is very close to the stopper in phase 2. The charge starts to flow and reaches the maximum transfer amount when the beam impacts the stopper. A positive voltage peak is generated due to the rapid change of the total capacitance at the impact moment. After that, the host beam enters phase 3. The beam segment from the support to the bluff body continues to move forward because of the inertia of the bluff body and the beam itself. The tribo-pair keeps engaged during this period, and there is no charge transformation through two electrodes, corresponding to zero voltage output. In phase 4, the host beam moves backward from the extreme position, and the tribo-pair starts to separate. The charge flows rapidly in the reverse direction, resulting in the generation of a negative voltage peak. Phase 1 to phase 4 constitutes one complete vibration cycle for generating an AC voltage by the harvester. The next voltage peak will occur until the host beam goes back to contact the stopper in the subsequent cycle. The simulated voltage signal agrees well with the acquired experimental voltage signal for GTEH-A working at a wind velocity of 10 m/s (Fig. 7(c)). Obviously, the proposed model can capture the actual physical features of the harvester.

6. Performance improvement and parametric study

It can also be observed from Fig. 7 that there is a relatively long time interval without voltage output between two voltage cycles and within one cycle (phase 3). During this interval, the motion of the host beam, i.e., the vibration energy, is not converted into

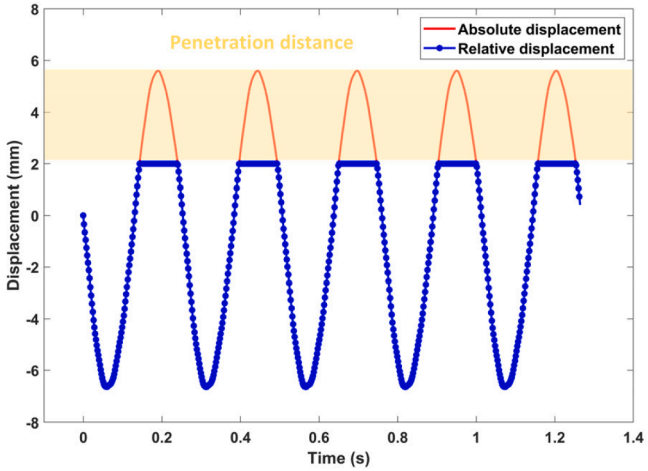

Fig. 6. Displacement of the beam at $x_1 = 80$ mm at the wind velocity of 10 m/s.

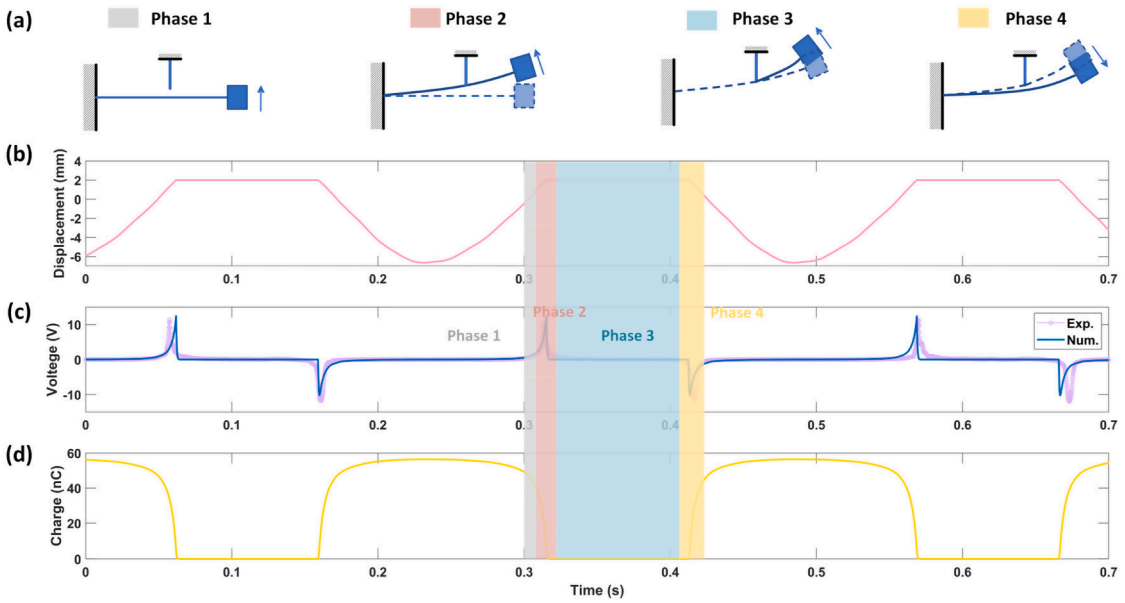

Fig. 7. Simulated displacements, voltage outputs, and charges at different phases of the impact-engaged galloping vibration process.

electricity. In order to achieve a higher energy conversion efficiency, it is necessary to shorten this time interval by either increasing the vibration frequency of the host beam or shortening the penetration distance (e.g., with a stiffer stopper). One advantage of the current GTEH design is that the gap distance can be easily tuned by adjusting the spacer. The frequency can also be varied by changing the cantilever beam, which also demonstrates the excellent design flexibility of the GTEH. For a beam structure, its natural frequency is related to its stiffness and mass, which can be modified by changing its geometric dimension. Considering that the host beam is self-excited due to the aerodynamic force, an extremely stiff beam cannot vibrate or only vibrate at very high wind velocity. In this regard, the selection of the beam stiffness should not sacrifice the cut-in wind velocity too much. Finally, the beam dimension is chosen to be 1 mm $\times$ 25 mm $\times$ 210 mm. The natural frequency increases from 4 Hz to 8.6 Hz, and the cut-in wind velocity becomes 3 m/s, which is acceptable for low wind velocity energy harvesting. In addition, as the proposed GTEH is based on the contact and separation of tribo-pair, the induced impact has a significant effect on the energy generation ability of the harvester. The impact is related to the gap distance, aerodynamic force, and contact stiffness. In order to further improve the harvester performance and provide some guidelines on the design of TEHs working on contact-separation mode, parametric studies concerning those factors are conducted based on GTEH-B since it shows the best performance in the preliminary test.

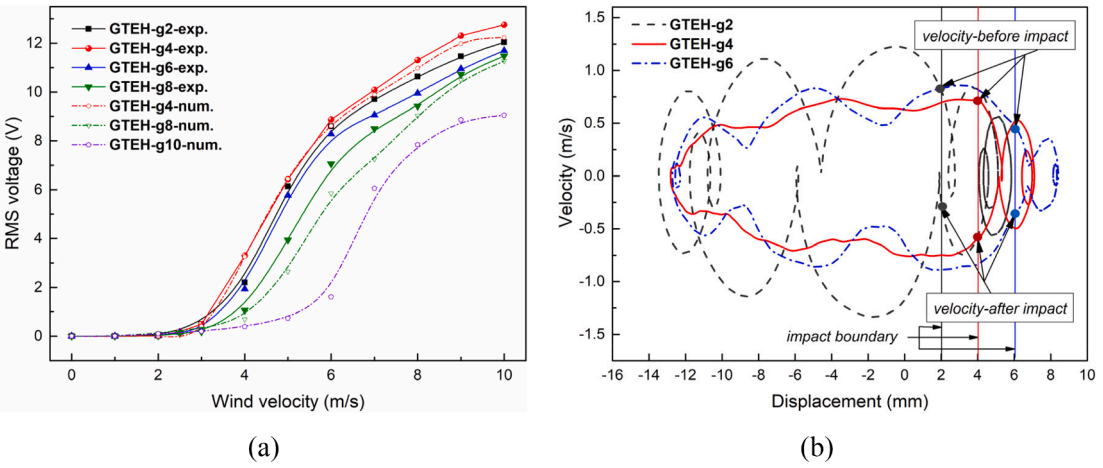

Fig. 8. (a) RMS voltage of GTEHs with various gap distances at different wind velocities; (b) Phase diagram for GTEH-g2, GTEH-g4 and GTEH-g6 obtained from simulation.

6.1. Gap distance

The gap distance between the middle plate and stopper may influence the energy generation ability of the GTEH because the speed of the middle plate approaching the stopper varies with the gap distances. GTEH-B is modified by replacing with the optimized beam, and the stopper remains unchanged. The gap distance is controlled by adjusting the thickness of the spacer. A new notion GTEH-gX is used for the harvesters, in which X represents the various gap distances (X = 2 mm, 4 mm, 6 mm, and 8 mm). The experimental results in Fig. 8(a) indicate the existence of an optimal gap distance for the GTEH. GTEH-g4 produces an V_{RMS} around 12.7 V at the wind velocity of 10 m/s. It can also reach up to 6.3 V at a wind velocity of 5 m/s, demonstrating its ability for low velocity wind energy harvesting. GTEH-g4 shows the best energy generation performance among all the harvesters that were tested in the experiment. Very narrow gaps, such as 1 mm or 0 mm, were not tested in this study, because initial contact within the tribo-pair could increase overall stiffness and natural frequency of the system, and the host beam cannot be self-excited if the middle plate initially contacts the stopper. GTEH-g2 and GTEH-g6 show similar voltage output that is lower than GTEH-g4. The difference can be attributed to the velocity of the beam before and after the impact with the stopper.

Fig. 8(b) shows the phase diagram for GTEHs with various gap distances from simulation. It is clear that the velocity before impact is larger than the velocity after impact for GTEH-g2 because the narrow gap allows the beam to impact the stopper at a relatively high speed, leading to a high energy loss and reduction of the velocity after impact. For GTEH-g4, the absolute velocities before and after the impact are almost the same, indicating less energy loss. Thus GTEH-g4 produces a considerably larger RMS voltage output than GTEH-g2, even though the velocity before the impact of GTEH-g4 is smaller than that of GTEH-g2. As for GTEH-g6, the large gap makes the beam impact the stopper with a low velocity thus generating a small voltage output. Numerical simulation of the proposed aero-electro-mechanical model presented in Section 3 was conducted as well. The numerical results for GTEH-g4 and GTEH-g8 show good agreement with the corresponding experimental results, even though the voltage output of GTEH-g8-num is smaller than that of GTEH-g8-exp. The post-fixes -num and -exp denote the numerical and experimental results, respectively. GTEH-g10 with a broader gap is modeled, and the result indicates that the gap is not recommended to be excessively tuned. Otherwise, the cut-in wind velocity of GTEH for generating electricity will increase. Therefore, there is an optimal gap distance for the proposed GTEH, and it needs to be carefully selected in actual applications.

6.2. Bluff body

The dimension of the bluff body, especially the exposed area, will affect the induced aerodynamic force. In order to investigate its influence, three bluff bodies with different heights (H = 110 mm, H = 130 mm, and H = 150 mm) are fabricated for testing. The cross-sectional dimension of the square cross-section is maintained at 40 mm × 40 mm. The bluff modification is based on the GTEH-g4. For a cantilever system, the change in dimension of the bluff body affects its tip mass, which influences the natural frequency of the host beam. The GTEH with the height of Y mm is noted as GTEH-HY. The weight of GTEH-H150 is 12.5 g. To eliminate the weight difference between bluff bodies, attachments are added to the other two harvesters to make their weight consistently being 12.5 g. Fig. 9 compares the RMS voltage from the experiment and simulation for the GTEHs with various bluff bodies. One clear trend is that V_{RMS} increases with the bluff body height, and such increment is more obvious at high wind velocities. The reason should be attributed to the growing aerodynamic force, which eases the contact of the tribo-pair at a relatively high speed leading to a faster charge transformation. The numerical results from the proposed model agree well with the experimental results, indicating the good accuracy of the aero-electro-mechanical model. The performance of GTEHs shows clearer discrepancies under the high wind velocity range from 8 m/s to 10 m/ s because of the induced impact. To this end, it is evident that a large bluff body benefits the performance of the harvester.

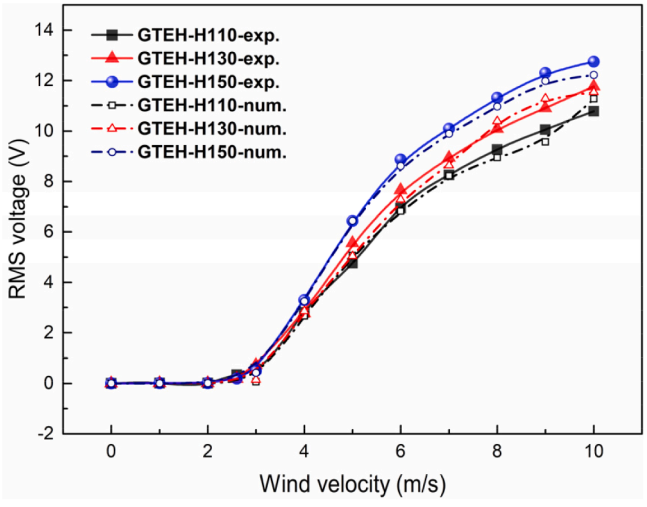

Fig. 9. Comparison between experimental and numerical results for GTEHs with bluff bodies having different heights.

However, it is also not recommended to use an oversized bluff body in view of miniaturization. Besides, beam rotation may happen if the bluff body is too high, which is not suitable for energy harvesting of GTEH.

6.3. Contact stiffness

For the harvester working on contact-separation mode, inevitable impact within the tribo-pair makes the host beam exhibit a particular nonlinear dynamic behavior. Hence, it is worthwhile to investigate the effect of contact stiffness on the performance of the GTEH. The contact stiffness is related to the contact speed, the material type, and the stopper's stiffness. In our test, the contact stiffness is adjusted by controlling the stiffness of the stopper. Basically, three stoppers with different thicknesses (3 mm, 6 mm, and 9 mm) are introduced. The parametric study is conducted based on GTEH-g4-H150. The harvesters with various stoppers are denoted as GTEH-KS, GTEH-KM and GTEH-KB. The post-fixes, namely, -KS, -KM, and -KB, respectively, indicate small, moderate, and big contact stiffness. As shown in Fig. 10**(a)**, increasing the contact stiffness reduces the V_{RMS}, and such a voltage drop is more overt at the high wind velocity region. It is observed that the AC voltage signal is highly asymmetric when the contact stiffness is large. Fig. 10(b) shows the positive voltage peak (V_{P-Peak}) obtained at various wind velocities for GTEHs with different contact stiffness. The three curves almost overlap with each other. The reason is that the approaching speed of the middle plate for various GTEHs are the same before impact, which results in similar charge transformation amount and speed, thus giving similar voltage output. However, the after-impact velocity of the host beam is diverse under various contact stiffness, which influences the charge transformation. Fig. 10**(c)** shows the negative voltage peak (V_{N-Peak}) of the tested GTEHs. V_{N-Peak} drops significantly when the contact stiffness increases, by comparing the output from KS, KM to KB. The contact of the tribo-pair changes from relatively soft impact to highly rigid impact from KS to KB. In such case, the host beam suffers an increasing energy loss with the growing contact stiffness, leading to the decrease of V_{N-Peak}. As a result, the peak-to-peak voltage (V_{P-P}) also decreases with the growing contact stiffness as shown in Fig. 10(d). Strong nonlinearity happens during the contact for rigid impact. The causing impulsive separation between contact surfaces could result in sporadic voltage output, which reduces the magnitude of the negative voltage peak and gives the asymmetric AC voltage signal. Such a

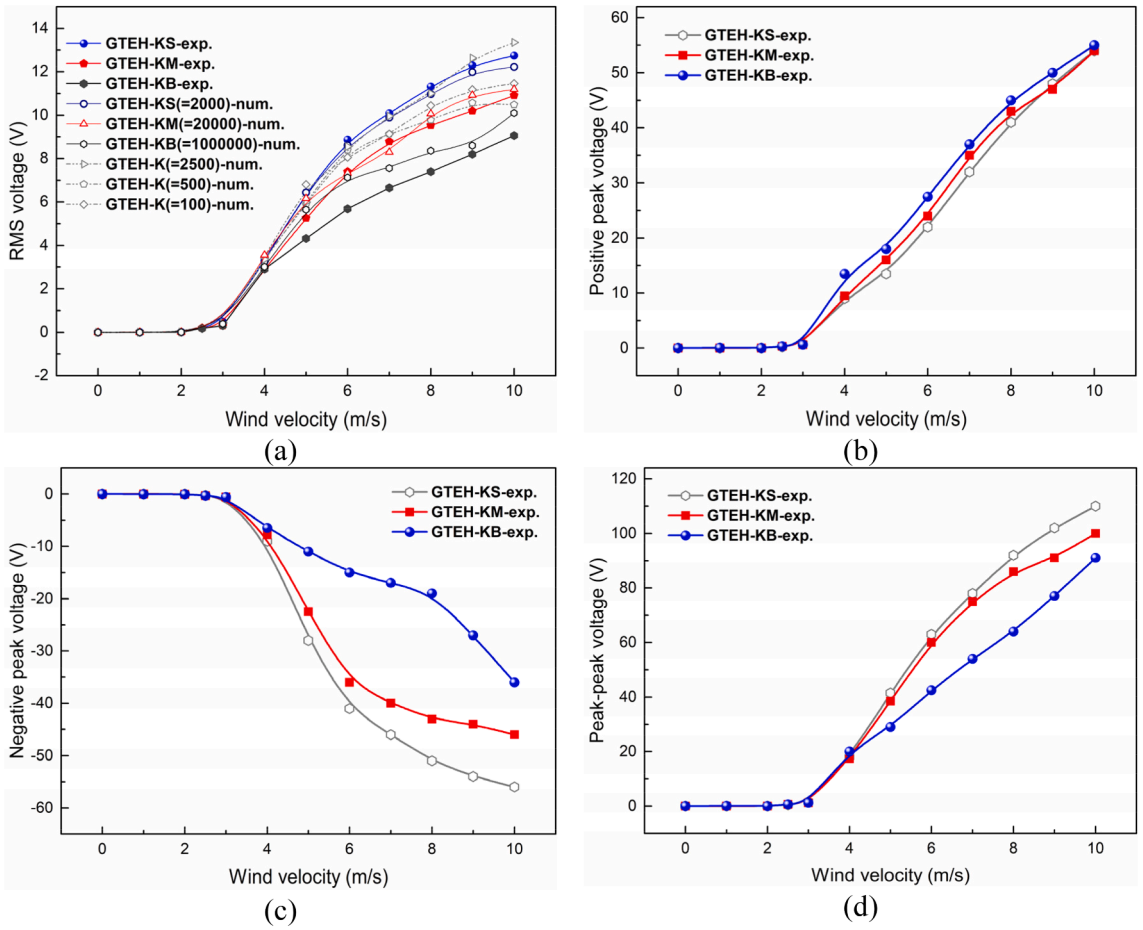

Fig. 10. (a) Comparison between experimental and numerical results for GTEH with various contact stiffness; (b) positive peak voltage; (c) negative peak voltage and (d) peak-to-peak voltage obtained for different GTEHs at various wind velocities.

phenomenon can be clearly observed in Fig. 11, which shows the actual voltage output for GTEHs with various stoppers at the wind velocity of 10 m/s from the experiment. Sporadically distributed irregular voltage peaks occur for highly rigid impact, such as GTEH-KB.

In order to fully understand the effect of the contact stiffness, numerical simulation is carried out using the proposed model. The determination of the contact stiffness during vibro-impact is not straight-forward. In this study, the contact stiffness specified in the model is estimated through the frequency response of the harvester. It is known that the natural frequency of the beam will increase due to its hardening behavior when impact happens, which could lead to the shift of the natural frequency. Such a behavior provides a method to estimate the induced contact stiffness for the vibro-impact system. The fundamental natural frequency of the beam is 8.6 Hz. In the experiment, the natural frequencies shift to 9.6 Hz, 10.0 Hz and 10.5 Hz for GTEH-KS, GTEH-KM and GTEH-KB, respectively, at the wind velocity of 10 m/s. By leveraging on this observation, the contact stiffness of GTEH-KS and GTEH-KM are determined to be 2000 N/m and 20000 N/m with the resulting simulated natural frequencies of 9.5 Hz and 9.9 Hz, which match well with the observed natural frequencies. As shown in Fig. 10(a), the numerical results for both harvesters agree well with the experimental results with reasonable disparity for GTEH-KM. However, even the KB is set to 1000000 N/m for GTEH-KB in the modeling, the obtained natural frequency is only 10.1 Hz, which is lower than the corresponding value from the experiment. Such a significant discrepancy for GTEH-KB could be due to the employed modeling method of impact. The FIM has low accuracy and efficiency in dealing with highly rigid impacts. To some extent, the proposed model can model the nonlinear impact behavior of GTEH from soft impact to moderately rigid impact. In order to further understand the validity of the proposed model, more contact stiffnesses with lower values (K = 100 N/m, 500 N/m and 2500 N/m) are tried out in simulation. The results indicate that too soft impact will not improve the energy generation ability of the harvester. There is an optimal contact stiffness for the current harvester design. Based on the analysis, the most efficient contact stiffness is around 2500 N/m for the current harvester design, giving an ideal V_{RMS} output at around 13 V.

This section has conducted a detailed parametric study, both experimentally and numerically, to investigate the effects of the bluff body, stopper, and gap distance on the energy harvesting performance. All these factors affect the contact stiffness between the middle plate and stopper. Proper contact benefits the charge transformation, leading to large electrical output. Nevertheless, a highly rigid contact causes tremendous energy loss and result in the reduction of V_{N-Peak}, as well as V_{RMS}. Among all these factors, adjusting the stopper stiffness is a direct method to tune the contact stiffness compared to changing bluff body and gap distance. The proposed model shows good accuracy in a broad range of contact stiffness even it loses its accuracy at extremely high contact stiffness. The optimal contact stiffness of GTEH locates in the moderate range. Hence, the proposed model can be used to design other TEHs working on the contact-separation mode.

7. Performance characterization

In actual application scenarios, the harvested energy needs to be stored in a battery or a capacitor first. Subsequently, the power management unit acquires a proper amount of energy to power small electronics. As discussed in the previous sections, GTEH-g4-H150-KS is close to the optimal configuration of the harvester. Thus, it is selected to examine the energy generation ability of the proposed harvester. In order to find the optimal power of the selected GTEH, the output of the harvester is connected to an adjustable resistor for impedance matching. The voltage of the resistor is measured when varying the resistance. Fig. 12 shows the power output from the harvester under different wind velocities. The maximum power is 290 μW at the wind velocity of 10 m/s. Even at a relatively lower wind velocity of 6 m/s, the maximum power could reach 196 μW. For the application demonstration of the proposed GTEH, the voltage that comes from the harvester is rectified to charge capacitors and light LEDs. The circuit is shown in Fig. 13(a). The wind velocity maintains at 9 m/s. Four capacitors with capacitance of 4.7 μF, 22 μF, 47 μF and 100 μF are chosen for the experiment. From Fig. 13**(b)**, the harvester can charge the capacitors to 22.3 V, 6.7 V, 3.3 V and 1.4 V in 60 s, respectively. The charging results prove that the harvester can supply sufficient energy to power sensors since the basic voltage requirement for most electronics is 3.6 V. In Fig. 13 **(c)**, the harvester can light up 40 LEDs even at a wind velocity of only 4 m/s, indicating the good capability of the proposed GTEH for low velocity wind energy harvesting. Furthermore, there is still a room to improve the energy generation performance of the proposed GTEH. For example, using surface treatment technology for the raw PTFE materials, such as plasma treatment and surface etching, can elevate the power output to a higher level [50,51].

8. Conclusion

In this study, a cantilever-type vibro-impact triboelectric energy harvester is proposed for wind energy harvesting based on the galloping effect of the bluff body. An aero-electro-mechanical model is formulated considering the aerodynamic force and the impact force. Prototypes of the GTEH are tested in the wind tunnel. The effects of critical design parameters such as the dimension of the bluff body, gap distance, and contact stiffness are systematically investigated. The actual performance of the GTEH is also examined experimentally. The main findings from this study are summarized as follows.

(1) The cantilever beam has a broad flexibility in harvester design. One challenge of using a cantilever beam for TEH working on contact separation mode is that the complete contact within tribo-pair is difficult to achieve. Non-complete contact of the tribo-pair leads to poor power output. The proposed harvester design provides a good solution to ensure complete contact by introducing a middle plate with one rotation degree of freedom, which is further applied in wind energy harvesting. Very low cut-in wind velocity (<4 m/s) of the GTEH demonstrates its ability for low wind velocity energy harvesting.

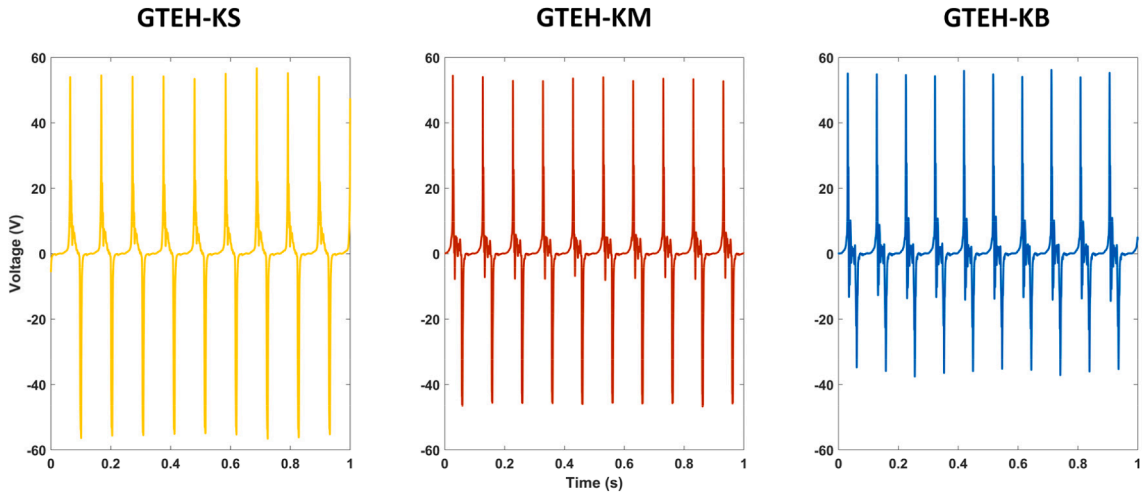

Fig. 11. Voltage outputs from GTEHs configured with different stoppers at the wind velocity of 10 m/s.

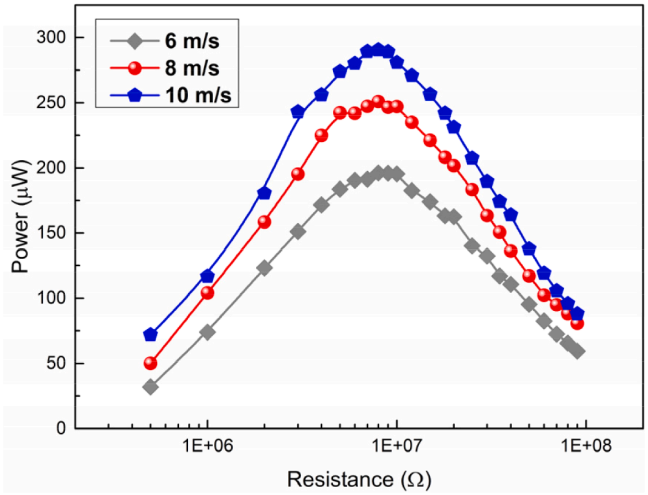

Fig. 12. Power output of GTEH-g4-H150-KS at various external resistances when exposed to different wind velocities.

(2) Impact between two contact surfaces of the tribo-pair is employed in the proposed GTEH. The contact status dominates the energy generation performance of the harvester. Unlike the traditional lumped parameter model, this paper has proposed a distributed parameter model concerning the coupled aero-electro-mechanical effect and the impact effect. The FIM is used to simulate the impact in the model. Natural frequency shift due to the impact can be captured by the model. Good agreement between the numerical and experimental results indicates the accuracy of the theoretical model, which provides a guideline for the modeling of TEHs working on the contact and separation mode.

(3) Abundant parametric studies are carried out experimentally and numerically. The contact stiffness has a more prominent influence on the energy generation performance of the harvester compared to the dimension of the bluff body and gap distance. An asymmetric voltage output can be observed when a huge impact happens. Strong nonlinearity and energy loss of the impact result in a remarkable drop-down of the negative voltage output in each cycle. However, proper impact facilitates the complete contact of the tribo-pair, thus positively affecting the harvester's performance. Therefore, the impact plays a critical role in the energy conversion performance of the harvester. A moderate gap distance and contact stiffness are more profitable for the proposed GTEH.

(4) The prototype of GTEH shows a maximum RMS voltage output of 12.8 V with an maximum power of 290 μW at the wind velocity of 10 m/s. It also has a broad bandwidth due to the natural frequency shift. The GTEH exhibits good performance in charging capacitors and lighting LEDs, demonstrating its potential as an energy generator to power electronics.

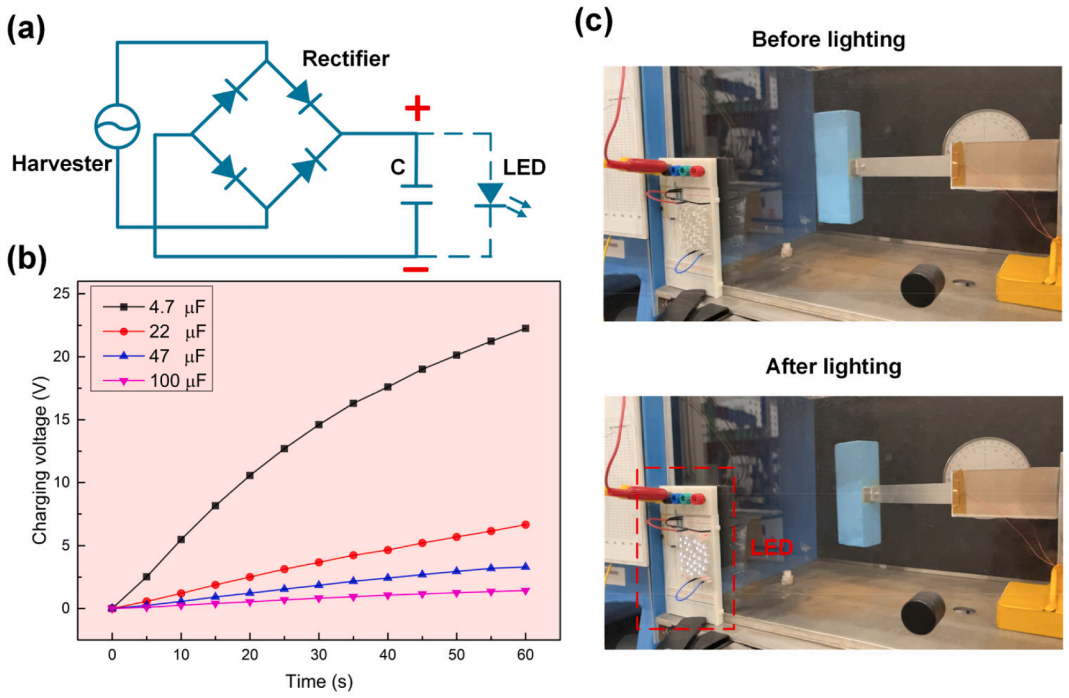

Fig. 13. (a) External circuit for charging capacitors and lighting LEDs; (b) capacitor charging curve for GTEH-B at a wind velocity of 9 m/s; (c) pictures of lighting 40 LEDs in the experiment.

CRediT authorship contribution statement

Chaoyang Zhao: Conceptualization, Methodology, Writing – original draft. **Guobiao Hu:** Investigation, Writing – review & editing. **Yaowen Yang:** Supervision, Writing – review & editing.

Declaration of Competing Interest

The authors declare that they have no known competing financial interests or personal relationships that could have appeared to influence the work reported in this paper.

References

[1] L.K. Wu, M. Jing, Y.L. Liu, H.M. Ning, X.Y. Liu, S.F. Liu, et al., Power generation by PVDF-TrFE/graphene nanocomposite films, Compos. Part B-Eng. 164 (2019) 703–709.
[2] L.K. Wu, W.F. Yuan, N. Hu, Z.C. Wang, C.L. Chen, J.H. Qiu, et al., Improved piezoelectricity of PVDF-HFP/carbon black composite films, J. Phys. D Appl. Phys. 47 (2014).
[3] L. Tang, Y. Yang, A nonlinear piezoelectric energy harvester with magnetic oscillator, Appl. Phys. Lett. 101 (2012).
[4] G. Hu, L. Tang, A. Banerjee, R. Das, Metastructure with piezoelectric element for simultaneous vibration suppression and energy harvesting, J. Vib. Acoust. 139 (2017).
[5] S. Wang, C. Wang, G. Yu, Z. Gao, Development and performance of a piezoelectric energy conversion structure applied in pavement, Energy Convers. Manage. 207 (2020).
[6] M.S.U. Rasel, J.-Y. Park, A sandpaper assisted micro-structured polydimethylsiloxane fabrication for human skin based triboelectric energy harvesting application, Appl. Energy 206 (2017) 150–158.
[7] F.R. Fan, L. Lin, G. Zhu, W. Wu, R. Zhang, Z.L. Wang, Transparent triboelectric nanogenerators and self-powered pressure sensors based on micropatterned plastic films, Nano Lett. 12 (2012) 3109–3114.
[8] S. Zargari, Z.D. Koozehkanani, H. Veladi, J. Sobhi, A. Rezania, A new Mylar-based triboelectric energy harvester with an innovative design for mechanical energy harvesting applications, Energy Convers. Manage. 244 (2021).
[9] S. Yong, J.Y. Wang, L.J. Yang, H.Q. Wang, H. Luo, R.J. Liao, et al., Auto-Switching Self-Powered System for Efficient Broad-Band Wind Energy Harvesting Based on Dual-Rotation Shaft Triboelectric Nanogenerator, Adv. Energy Mater. 14 (2021).
[10] J.Y. Wang, W.B. Ding, L. Pan, C.S. Wu, H. Yu, L.J. Yang, et al., Self-powered wind sensor system for detecting wind speed and direction based on a triboelectric nanogenerator, ACS Nano 12 (2018) 3954–3963.
[11] C.L. Zhao, Q. Zhang, W.L. Zhang, X.Y. Du, Y. Zhang, S.B. Gong, et al., Hybrid piezo/triboelectric nanogenerator for highly efficient and stable rotation energy harvesting, Nano Energy 57 (2019) 440–449.
[12] L. Bu, Z. Chen, Z. Chen, L. Qin, F. Yang, K. Xu, et al., Impact induced compound method for triboelectric-piezoelectric hybrid nanogenerators to achieve Watt level average power in low frequency rotations, Nano Energy 70 (2020).
[13] J. Bae, J. Lee, S. Kim, J. Ha, B.S. Lee, Y. Park, et al., Flutter-driven triboelectrification for harvesting wind energy, Nat. Commun. 5 (2014) 4929.
[14] L. Zhang, B. Zhang, J. Chen, L. Jin, W. Deng, J. Tang, et al., Lawn structured triboelectric nanogenerators for scavenging sweeping wind energy on rooftops, Adv. Mater. 28 (2016) 1650–1656.

[15] M. Perez, S. Boisseau, M. Geisler, P. Gasnier, J. Willemin, G. Despesse, et al., Aeroelastic flutter energy harvesters self-polarized by triboelectric effects, Smart Mater. Struct. 27 (2018).
[16] M. Perez, S. Boisseau, P. Gasnier, J. Willemin, J.L. Reboud, An electret-based aeroelastic flutter energy harvester, Smart Mater. Struct. 24 (2015).
[17] H. Phan, D.M. Shin, S.H. Jeon, T.Y. Kang, P. Han, G.H. Kim, et al., Aerodynamic and aeroelastic flutters driven triboelectric nanogenerators for harvesting broadband airflow energy, Nano Energy 33 (2017) 476–484.
[18] Y. Yang, Z.L. Wang, Triboelectric nanogenerator for harvesting wind energy and as self-powered wind vector sensor system, ACS Nano (2013).
[19] Z.F. Zhao, X. Pu, C.H. Du, L.X. Li, C.Y. Jiang, W.G. Hu, et al., Freestanding flag-type triboelectric nanogenerator for harvesting high-altitude wind energy from arbitrary directions, ACS Nano 10 (2016) 1780–1787.
[20] J. Wang, S. Zhou, Z. Zhang, D. Yurchenko, High-performance piezoelectric wind energy harvester with Y-shaped attachments, Energy Convers. Manage. 181 (2019) 645–652.
[21] L. Zhao, Y. Yang, An impact-based broadband aeroelastic energy harvester for concurrent wind and base vibration energy harvesting, Appl. Energy 212 (2018) 233–243.
[22] G.B. Hu, J.L. Wang, L.H. Tang, A comb-like beam based piezoelectric system for galloping energy harvesting, Mech. Syst. Sig. Process. 150 (2021).
[23] L. Zhang, B. Meng, Y. Xia, Z. Deng, H. Dai, P. Hagedorn, et al., Galloping triboelectric nanogenerator for energy harvesting under low wind speed, Nano Energy 70 (2020).
[24] Q. Wang, H.-X. Zou, L.-C. Zhao, M. Li, K.-X. Wei, L.-P. Huang, et al., A synergetic hybrid mechanism of piezoelectric and triboelectric for galloping wind energy harvesting, Appl. Phys. Lett. 117 (2020).
[25] B. Yang, W. Zeng, Z.-H. Peng, S.-R. Liu, K. Chen, X.-M. Tao, A fully verified theoretical analysis of contact-mode triboelectric nanogenerators as a wearable power source, Adv. Energy Mater. 6 (2016) 1600505.
[26] S. Niu, S. Wang, L. Lin, Y. Liu, Y.S. Zhou, Y. Hu, et al., Theoretical study of contact-mode triboelectric nanogenerators as an effective power source, Energy Environ. Sci. 6 (2013).
[27] J. Shao, M. Willatzen, Z.L. Wang, Theoretical modeling of triboelectric nanogenerators (TENGs), J. Appl. Phys. 128 (2020).
[28] A. Ibrahim, A. Ramini, S. Towfighian, Experimental and theoretical investigation of an impact vibration harvester with triboelectric transduction, J. Sound Vib. 416 (2018) 111–124.
[29] Y. Fu, H. Ouyang, R.B. Davis, Triboelectric energy harvesting from the vibro-impact of three cantilevered beams, Mech. Syst. Sig. Process. 121 (2019) 509–531.
[30] Y. Yang, L. Zhao, L. Tang, Comparative study of tip cross-sections for efficient galloping energy harvesting, Appl. Phys. Lett. 102 (2013).
[31] F. Ewere, G. Wang, B. Cain, Experimental investigation of galloping piezoelectric energy harvesters with square bluff bodies, Smart Mater. Struct. 23 (2014).
[32] A. Abdelkefi, M.R. Hajj, A.H. Nayfeh, Piezoelectric energy harvesting from transverse galloping of bluff bodies, Smart Mater. Struct. 22 (2013).
[33] J. Wang, L. Tang, L. Zhao, Z. Zhang, Efficiency investigation on energy harvesting from airflows in HVAC system based on galloping of isosceles triangle sectioned bluff bodies, Energy 172 (2019) 1066–1078.
[34] M.P. Païdoussis, S.J. Price, E. de Langre, Fluid-Structure Interactions - Cross-Flow-Induced Instabilities, Cambridge University Press, 2010.
[35] K. Yang, J. Wang, D. Yurchenko, A double-beam piezo-magneto-elastic wind energy harvester for improving the galloping-based energy harvesting, Appl. Phys. Lett. 115 (2019).
[36] J. Wang, L. Geng, S. Zhou, Z. Zhang, Z. Lai, D. Yurchenko, Design, modeling and experiments of broadband tristable galloping piezoelectric energy harvester, Acta Mech. Sin. 36 (2020) 592–605.
[37] C.Y. Zhao, Y.W. Yang, D. Upadrashta, L.Y. Zhao, Design, modeling and experimental validation of a low-frequency cantilever triboelectric energy harvester, Energy 214 (2021).
[38] H.C. Tsai, M.K. Wu, Methods to compute dynamic response of a cantilever with a stop to limit motion, Comput. Struct. 58 (1996) 859–867.
[39] C. Wang, J. Kim, New analysis method for a thin beam impacting against a stop based on the full continuous model, J. Sound Vib. 191 (1996) 809–823.
[40] E.K. Ervin, J.A. Wickert, Repetitive impact response of a beam structure subjected to harmonic base excitation, J. Sound Vib. 307 (2007) 2–19.
[41] K.J.L. Fegelman, K. Grosh, Dynamics of a flexible beam contacting a linear spring at low frequency excitation: experiment and analysis, J. Vibrat. Acoust. Trans. ASME 124 (2002) 237–249.
[42] D.J. Wagg, S.R. Bishop, A note on modelling multi-degree-of-freedom vibro-impact systems using coefficient of restitution models, J. Sound Vib. 236 (2000) 176–184.
[43] C.P. Vyasarayani, J. McPhee, S. Birkett, Modeling impacts between a continuous system and a rigid obstacle using coefficient of restitution, J. Appl. Mech. Trans. ASME 77 (2010).
[44] A. Erturk, D.J. Inman, A distributed parameter electromechanical model for cantilevered piezoelectric energy harvesters, J. Vib. Acoust. 130 (2008).
[45] R.W. Clough, J. Penzien, Dynamics of Structures, Wiley, New York, 1975.
[46] A. Barrero-Gil, G. Alonso, A. Sanz-Andres, Energy harvesting from transverse galloping, J. Sound Vib. 329 (2010) 2873–2883.
[47] Erturk AI, D. J. Mechanical Considerations for Modeling of Vibration-based Energy Harvesters. Proceedings of the ASME IDETC 21st Biennial Conference on Mechanical Vibration and Noise. 2007;4-7 September 2007.
[48] A. Erturk, D.J. Inman, On mechanical modeling of cantilevered piezoelectric vibration energy harvesters, J. Intell. Mater. Syst. Struct. 19 (2008) 1311–1325.
[49] S.M. Niu, Z.L. Wang, Theoretical systems of triboelectric nanogenerators, Nano Energy 14 (2015) 161–192.
[50] X.L. Cheng, B. Meng, X.X. Chen, M.D. Han, H.T. Chen, Z.M. Su, et al., Single-step fluorocarbon plasma treatment-induced wrinkle structure for high-performance triboelectric nanogenerator, Small. 12 (2016) 229–236.
[51] Z. Fang, K.H. Chan, X. Lu, C.F. Tan, G.W. Ho, Surface texturing and dielectric property tuning toward boosting of triboelectric nanogenerator performance, J. Mater. Chem. A 6 (2018) 52–57.